Available online at www.sciencedirect.com

SciVerse ScienceDirect

Solar Energy 88 (2013) 182–191

SOLAR ENERGY

www.elsevier.com/locate/solener

Enhanced performance of solar-driven photovoltaic–thermoelectric hybrid system in an integrated design

Yuan Deng *, Wei Zhu, Yao Wang, Yongming Shi

Beijing Key Laboratory for Advanced Functional Materials and Thin Film Technology, School of Material Science and Engineering, Beihang University, Beijing 100191, China

Received 15 June 2012; received in revised form 30 November 2012; accepted 1 December 2012
Available online 3 January 2013

Communicated by: Associate Editor Mukund Patel

Abstract

A solar-driven hybrid generation system (HGS) in an integrated design is successfully fabricated, which consists of a silicon thin-film solar cell (STC), thermoelectric generators (TEGs) and a heat collector. STC absorbs parts of the solar energy and directly converts it into electric energy. The undesired waste heat from STC and parts of the solar energy are collected by the heat collector and conducted to TEG to produce thermoelectric conversion. The structure and the performance of HGS are discussed. A numerical simulation is also performed on TEG to obtain the distribution of heat flux using finite element method (FEM). The results show that the performances of TEG and STC are synchronously enhanced due to the integrated design. Especially the heat flux on the hot side of TEG integrated in HGS increases by more than tenfold. The total generated power of 393 mW is obtained in HGS, which is twice larger than that of single STC. The developed HGS is a promising power system which can effectively broaden the use of the solar spectrum and increase the power output in solar conversion.

Keywords: Solar energy; Hybrid generation system; Silicon thin-film cell; Thermoelectric generator; Finite element method

1. Introduction

The efficient use of solar energy has been given priority to address energy and environment issues (Crowley, 2000; Yang and Yin, 2011). Photovoltaic (PV) technology is one of the highly competitive technologies to convert the incident solar radiation into electric energy. Silicon thin-film solar cell (STC) is developing rapidly in recent years for its natural abundance, environmental safety, potential high performance and capability of the low cost STC-production (Kondo and Matsuda, 2004; Yamamoto et al., 2004). To date, their stable efficiency is currently reported up to 9.5% in the lab (Aberle, 2009). Pursuing high efficiency is always the core task for PV technology. However, it is still far from being competitive with fossil fuel based energy conversion technologies. A major issue lies in the limited efficiency of solar energy conversation, for the STC can only absorb solar light up to 800 nm which results in the difficulty of fully utilizing the solar spectrum. What's worse, the majority of infrared energy is converted into waste heat and the temperature rise of STC leads to efficiency lost for the reduction of the open-circuit voltage and the lifetime. Therefore, it is important for STC to remove the waste heat and control the operating temperature.

Thermoelectric generator (TEG) can directly convert thermal energy into electric power, so it provides another way to use solar radiation and waste heat (Amatya and Ram, 2010; Li et al., 2010; Deng and Liu, 2009; Chen, 1996; Hsu et al., 2011; He et al., 2011). It is important to

* Corresponding author. Tel.: +86 010 82313482; fax: +86 010 82339431.
E-mail address: dengyuan@buaa.edu.cn (Y. Deng).

0038-092X/$ - see front matter © 2012 Elsevier Ltd. All rights reserved.
http://dx.doi.org/10.1016/j.solener.2012.12.002

Nomenclature

A	area (m^2)
C	specific heat capacity (J/Kg K)
D	electric flux density (C/m^2)
E	electric field intensity (V/m)
FF	fill factor
G	irradiance intensity (W)
I	current (A)
J	electric current density (A/m^2)
L	irradiance density (W/m^2)
P	power output (W)
Q	thermal input (W)
q	thermal flux (W/m^2)
$\dot{q}$	heat generation rate per unit volume (W/m^3)
R_l	electric load (Ω)
R_0	internal resistance (Ω)
T	temperature (K)
V	voltage (V)

Greek symbols

ρ	density (kg/m^3)
α	seebeck coefficient (V/K)
κ	thermal conductivity (W/m K)
σ	electric conductivity (S/m)
ϕ	electric scalar potential (V)
η	efficiency
Δ	temperature difference (K)

Subscripts

c	cold side
h	hot side
max	maximum
oc	open-circuit
op	optimum
sc	short-circuit
tot	total

keep a significant temperature difference across the TEG under solar radiation (Kraemer et al., 2011). Many methods have been developed to increase the heat flux on TEG with an optical concentrator (Li et al., 2010; Chow, 2010; Omer and Infield, 2000) or to enhance the thermoelectric transport properties (Chen et al., 2003). Reasonable numerical simulation and thermal design are also important to predict the generating performance. Xiao et al. (2011) established a three-dimensional finite element model of multi-stage thermoelectric generator module for performance optimization. Ju et al. (2012) presented a numerical analysis and optimization of a spectrum splitting photovoltaic–thermoelectric hybrid system under concentrations.

In recent years, photovoltaic and thermoelectric hybrid generation system has gained wide attention (Rockendorf et al., 1999; Muhtaroglu et al., 2008; Van Sark, 2011; Kraemer et al., 2008; Vorobiev et al., 2006; Ju et al., 2012; Chavez-Urbiola et al., 2012). The TEG was directly placed under the solar cell in order to use the remaining waste heat, and the total efficiency might be around 30% according to the theoretical calculation (Vorobiev et al., 2006). Van Sark (2011) presented a simple model for the calculation of the PV/TE hybrid device and demonstrated its usefulness for energy conversion in the world sun-belt area. Chavez-Urbiola et al. (2012) discussed the efficiency of solar hybrid system at different operation modes and the cost of the hybrid system. Guo et al. (2010) and Wang et al. (2011) found that the efficiency of the hybrid system comprising dye-sensitized solar cell (DSC) and thermoelectric generator could rise to about 13% compared with that of single PV.

However, there are still some challenges about the development of the hybrid system. Such as, the energy of irradiation is not fully used due to the large heat loss through air convection; the temperature difference across TEG model is still relatively low. Here, a novel hybrid generation system is developed through an integrated design to achieve higher power generation. This HGS consists of a silicon thin-film solar cell, thermoelectric generators and a heat collector. An absorbing layer is introduced to collect thermal energy, and an insulation layer and a conducting layer are used to prevent heat loss and ensure effective heat conduction respectively. By optimizing the heat collector design in HGS, a larger temperature difference has been obtained across TEG. Also, a numerical simulation is performed on the TEG using finite element method (FEM) to obtain its heat-flux distribution. Finally, cost analysis of this HGS configuration is conducted to estimate the economic feasibility.

2. Experimental and constitutive equations

2.1. Fabrication of HGS

Fig. 1a and b is a schematic illustration and physical photographs of the HGS, respectively. The size of TEG module is 40 mm × 40 mm × 3.7 mm. STC module is amorphous silicon thin-film cell with the size of 170 mm × 40 mm × 1 mm. A bowl-shaped heat collector with an absorbing layer, a conducting layer and an insulation layer was integrated in the HGS. Copper foil was fabricated to a bowl shape to conduct heat to TEG. It was also stuck to the side and back of STC to accelerate the heat conduction. The black polymer tape covered on the surface of copper foil was used as the absorbing layer to absorb the solar heat. Next, four TEGs were attached to the copper foil on the back of STC. Then, a layer of foam polymer was stuck to the back of copper foil as the insulation layer. Finally, aluminum fin heat sinks were affixed to the cold-side of TEGs for heat dissipation.

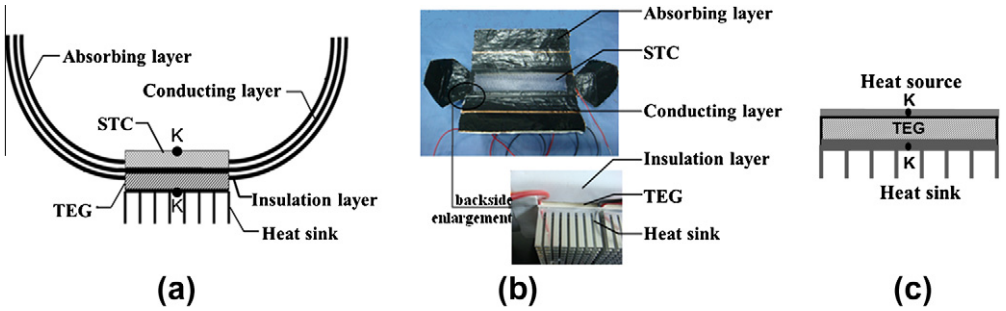

Fig. 1. (a) Schematic illustration of HGS, (b) Physical photographs of HGS and (c) A sketch of the location of thermometer on TEG for measuring heat source and sink temperatures.

In order to determine the generation characteristic of TEG, a heating plate was used as heat source and an aluminum fin was attached to the backside of TEG as heat sink. The temperatures were measured ("K" in Fig. 1c) to obtain the temperature difference across the both sides of TEG. Before the measurements, both sides of TEG were coated with silicone grease to reduce thermal resistivity. Besides, when TEG was assembled with STC and the heat collector, the location of thermometer for measuring temperature was shown in Fig. 1a. The temperature of STC is also supposed as the hot-side temperature of TEG, since the thickness of STC is very small.

2.2. Characterization and measurements

The solar simulation device (CMH-250 Metal Halide Lamp) was used in measurement. The intensity of illumination was recorded by FZ-A irradiatometer. The intensity of outdoor solar radiation was obtained by Newport 842-PE optical power and energy meter. The incident photon to electricity performance (voltage–current curve) was measured and recorded by CHI630A electrochemical workstation. The UT33B multimeter was used to measure the open-circuit voltage and short-circuit current of cells. UT320 Digital Thermometers was used to record the temperature. All the tests were taken under illumination intensity of 60 mW/cm^2.

2.3. Governing equations in thermoelectric analysis

In thermoelectric analysis, the commercial software ANSYS based on finite element analysis is used. The equations of heat flow and electric charge are expressed as:

$$\rho C\frac{\partial T}{\partial t}+\nabla\cdot\vec{q}=\dot{q} \tag{1}$$

$$\nabla\cdot\left(\vec{J}+\frac{\partial\vec{D}}{\partial t}\right)=0 \tag{2}$$

where ρ, C, T, $\vec{q}$ and $\dot{q}$ stand for density, specific heat capacity, absolute temperature, heat flux vector and heat generation rate per unit volume, respectively. $\vec{J}$ is the electric current density vector and $\vec{D}$ is the electric flux density vector.

The above two equations are coupled by the set of thermoelectric constitutive equations (Antonova and Looman, 2005):

$$\vec{q}=\alpha T\vec{J}-\kappa\nabla T \tag{3}$$

$$\vec{J}=\sigma(\vec{E}-\alpha\nabla T) \tag{4}$$

where α, κ, σ are respectively seebeck coefficient, thermal conductivity and electrical conductivity. $\vec{E}=-\nabla\phi$ is the electric field intensity vector and ϕ is the electric scalar potential. The displacement current $\frac{\partial\vec{D}}{\partial t}$ associated with the capacitive effects plays an unimportant role unless fast transient processes are considered. Therefore, in the steady-state model, the Eqs. (1) and (2) can be simplified into the following general forms:

$$\nabla\cdot\vec{q}=\dot{q} \tag{5}$$

$$\nabla\cdot\vec{J}=0 \tag{6}$$

Substituting Eqs. (3) and (4) into Eqs. (5) and (6) produces a system of coupled equations of thermoelectricity:

$$\nabla\cdot(\alpha T\vec{J})-\nabla\cdot(\kappa\nabla T)=\dot{q} \tag{7}$$

$$\nabla\cdot(\sigma\alpha\nabla T)+\nabla\cdot(\sigma\nabla\phi)=0 \tag{8}$$

Then, the numerical simulation was performed by using the ANSYS to conduct electro-thermal multiphysics analyses.

3. Results and discussion

3.1. Heat absorption and dissipation

STC mainly absorbs visible solar radiation and exhausts waste heat. The majority of infrared energy and undesired waste heat were collected by the designed heat collector and conducted to TEG to give a thermoelectric conversion. A bowl-shaped heat collector with an absorbing layer, a conducting layer and an insulation layer was integrated in the HGS. Copper foil was fabricated into a bowl shape to conduct heat to TEG. The black polymer tape was covered on the surface of copper foil as the absorbing layer to absorb the solar heat. The bowl-shaped heat collector with the high-efficiency absorbing layer is beneficial to absorb the sun light. Meanwhile the copper foil is in favor of heat

Table 1
Performance of TEG in HGS with different absorbing layers and cooling ways as natural cooling(I) or water cooling(II).

Absorbing layers	V_{oc} (V)		I_{sc} (mA)		P_{max} (mW)		FF	
	I	II	I	II	I	II	I	II
None	0.023	0.035	7.64	11.67	0.042	0.099	0.239	0.242
Graphite	0.049	0.072	16.33	25.67	0.184	0.454	0.230	0.246
Optical–thermal thin film	0.054	0.083	17.56	24.79	0.213	0.501	0.225	0.243
Black polymer tape	0.054	0.080	15.99	28.66	0.199	0.525	0.230	0.229

dissipation to the hot side of TEG. It is the key to keep large temperature difference across the TEG, which depends on heat absorption capability of the hot side and heat dissipation capability of the cold side. The type of heat absorbing layers (graphite, optical–thermal thin film, black polymer tape) and cooling ways (water cooling and natural cooling) have large effect on the performance of TEG. The performances of TEG under different work conditions are shown in Table 1.

Without the absorbing layer on the surface of the heat collector, heat absorption is not effective. Only a small temperature difference across the TEG is obtained, and the open-circuit voltage is only 0.023 V at natural cooling. When the absorbing layer is loaded, the solar energy can be absorbed by the absorbing layer and translated into heat at high efficiency. And heat absorption is more effective to produce higher temperature difference across the TEG. The open-circuit voltage of TEG rises largely to about 0.054 V at natural cooling, over twice larger than that of TEG without the use of absorbing layer. The open-circuit voltage, the short-circuit current and the combined maximum output power of TEG covered with black polymer tape are almost the same as those of optical-thermal thin film layer. Therefore, black polymer tape is chosen as the absorbing layer to capture solar energy heat.

The cooling methods at cold side of TEG also affect the heat dissipation capability. Water cooling is used to maintain TEG's cold side at a low temperature. When the cooling method is changed from nature cooling to water cooling, larger temperature difference across the TEG is obtained to give much higher open-circuit voltage and short-circuit current. The results from Table 1 show that the heat can be timely taken away from the TEG's cold side owing to the use of water cooling. The fill factor FF of TEG can be figured out through Eq. (1) with an average value of 0.242.

$$FF = \frac{V_{op}I_{op}}{V_{oc}I_{sc}} = \frac{P_{max}}{V_{oc}I_{sc}} \tag{9}$$

where FF is the fill factor, V_{op} is the optimum working voltage, I_{op} is the optimum working current, V_{oc} is the open-circuit voltage and I_{sc} is the short-circuit current, P_{max} stands for the maximum power output.

3.2. Performance of STC

Because of the different generating behaviors between STC and TEG, the connection ways of STC and TEG affect the output performance of HGS. When STC and TEG are connected in series, the open-circuit voltage of HGS is the sum of every module's voltage. But the overall current output depends on the smaller one of TEG and STC (Guo et al., 2010). To avoid the loss of electric energy produced by STC and TEG, it is often stored in different rechargeable batteries or super-capacitors and then used after an electricity regulation (Yu et al., 2008).

Firstly, STC module with the illuminate area of 170 mm × 40 mm was placed under the sun exposure. The environment temperature is 310 K and the illumination intensity is 60 mW/cm^2. As shown in Fig. 2, when the single STC works under the illumination of solar simulation, it generates an open-circuit voltage of about 2.06 V and a short-circuit current of 0.21 A. With the solar illumination going on and the accumulation of waste heat on STC, the temperature of STC gradually rises up to 321 K. Meanwhile, the open-circuit voltage of STC decreases from 2.06 V to 1.93 V. As it was mentioned, the high temperature of STC would lead to the reduction of the open-circuit voltage. Then, the STC is integrated with TEG and the heat collector and is also illuminated under solar simulation. The open-circuit voltage yielded by STC begins to rise again immediately and finally keeps at 2.07 V in stable (see Fig. 2). This phenomenon shows that the undesired waste heat from STC is collected by the heat collector and conducted to TEG. The waste heat is removed and STC returns to the good working condition. During the whole work, the short-circuit current generated by STC keeps stable with I_{sc} of about 0.22 A. The above results indicate that the performance of STC is promoted

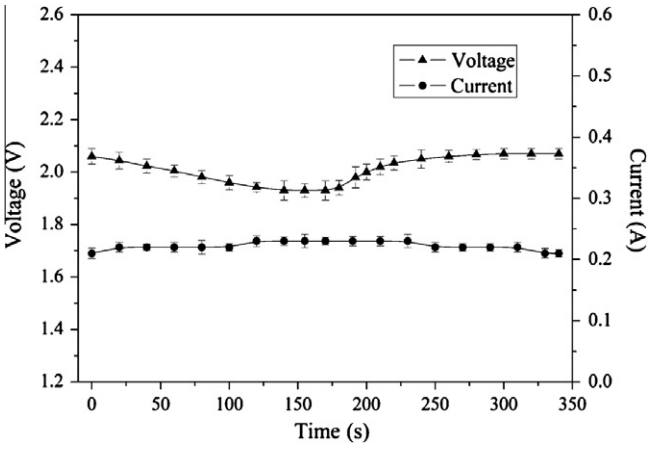

Fig. 2. The relationship of performance of STC with illuminated time, where STC is integrated in HGS after 170 s.

due to the integrated design with TEG and the heat collector in HGS.

3.3. Performance of TEG

Fig. 3 shows the performance of TEG with the illumination intensity of 60 mW/cm^2. When the single TEG works under the solar illumination, it only generates a stable open-circuit voltage of about 0.30 V and a short-circuit current of 0.024 A. When TEG is integrated with STC and the heat collector, which is also illuminated under the same solar irradiation from 22 s shown in Fig. 3, the open-circuit voltage and the short-circuit current produced by TEG rise sharply to the maximum of 3.25 V and 0.26 A, respectively. The temperature difference across the TEG is now 27 K, which is obtained from the generation characteristic of TEG. In HGS, the heat absorbed by heat collector is transferred to the hot side of TEG by copper foil, and meanwhile the water cooling with a strong cooling capacity takes the heat away from the cold side. Hence, a large temperature difference is formed across the TEG. Subsequently, the open-circuit voltage and short-circuit current decrease gradually and maintain stable values ($V_{oc} = 0.86$ V; $I_{sc} = 0.07$ A; $\triangle T = 7$ K). That is because the heat circulation comes back to a balance which leads to a decrease of the heat flux as well as the temperature difference. However, comparing the initial generating results with the final generating results of TEG, both open-circuit voltage and short-circuit current are enhanced largely from 0.30 V to 0.86 V and 0.024 A to 0.07 A, respectively. It can be obtained that the performance of TEG is also improved owing to the integrated design with STC and the heat collector in HGS.

3.4. Numerical simulation of TEG

3.4.1. Geometric model

The HGS consists of the STC, TEG and the heat collector. Among them, TEG is a major component which can use the waste heat to produce auxiliary thermoelectric conversion. The design of heat collector can effectively improve the performance of TEG as mentioned above. In order to obtain the distribution of heat flux on TEG under different operating conditions, the commercial software ANSYS based on finite element analysis is used to conduct thermoelectric analyses. Normally, a pair of thermoelectric unicouple assembly is considered as a unit for performance estimation. As shown in Fig. 4a, the scheme of the FEM model of TEG is comprised of ceramic substrate, copper strip and thermoelectric unicouple. Fig. 4b indicates the geometric size of the unicouple. The material properties such as seebeck coefficient, thermal conductivity, resistivity, density and heat capacity are all constant, which are summarized in Table 2.

3.4.2. Boundary conditions

The first boundary condition is applied to the hot side and cold side of TEG model and the temperatures are given by

$$T(z = 0) = T_c \quad \text{and} \quad T(z = 4.96) = T_h \tag{10}$$

In the meantime, heat loss along the side surfaces of the model is ignored. This implies

$$\frac{\partial T}{\partial x} = 0 \quad \text{and} \quad \frac{\partial T}{\partial y} = 0 \tag{11}$$

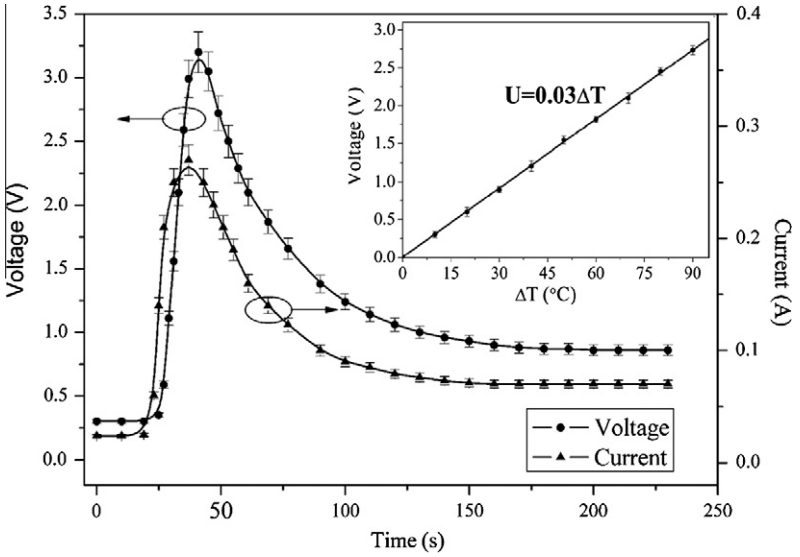

Fig. 3. The relationship of performance of TEG with illuminated time, where TEG is integrated in HGS after 22 s; the inset shows the generation characteristic of TEG.

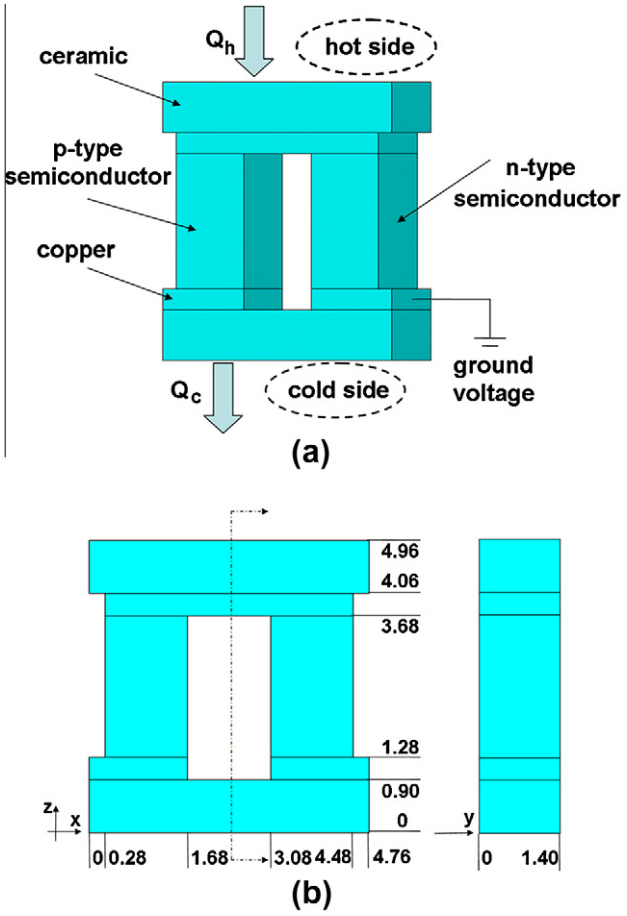

Fig. 4. (a) Scheme of the FEM model and (b) dimensions (mm).

Table 2
Thermoelectric properties for the FEM analysis.

Material properties	Seebeck coefficient (V/K)	Resistivity (Ωm)	Thermal conductivity (W/m K)	Density (kg/m^3)	Heat capacity (J/kg K)
n-Type material	−180e−6	2e−5	1.4	7740	154.4
p-Type material	180e−6	2e−5	1.4	7740	154.4
Copper strip	6.5e−6	1.67e−8	400	8920	385
Ceramic	–	–	31	3980	880

3.4.3. Output power and thermal flux of TEG

The output power is defined as follows:

$$P = I^2 R_l \tag{12}$$

where I and R_l stand for electric current and electric resistance, respectively. Generally, when output power is maximum, electric resistance is equal to the internal resistance of TEG. And the current can be calculated as

$$I = \frac{\alpha \Delta T}{R_0 + R_l} \tag{13}$$

where R_0 is the internal resistance. So the thermal input Q_h and thermal flux q_h to the hot side are obtained by

$$Q_h = \alpha T_h I - \frac{1}{2} I^2 R_0 + \kappa \Delta T \quad \text{and} \quad q_h = \frac{Q_h}{A_h} \tag{14}$$

where A_h stands for the hot-side area of TEG model.

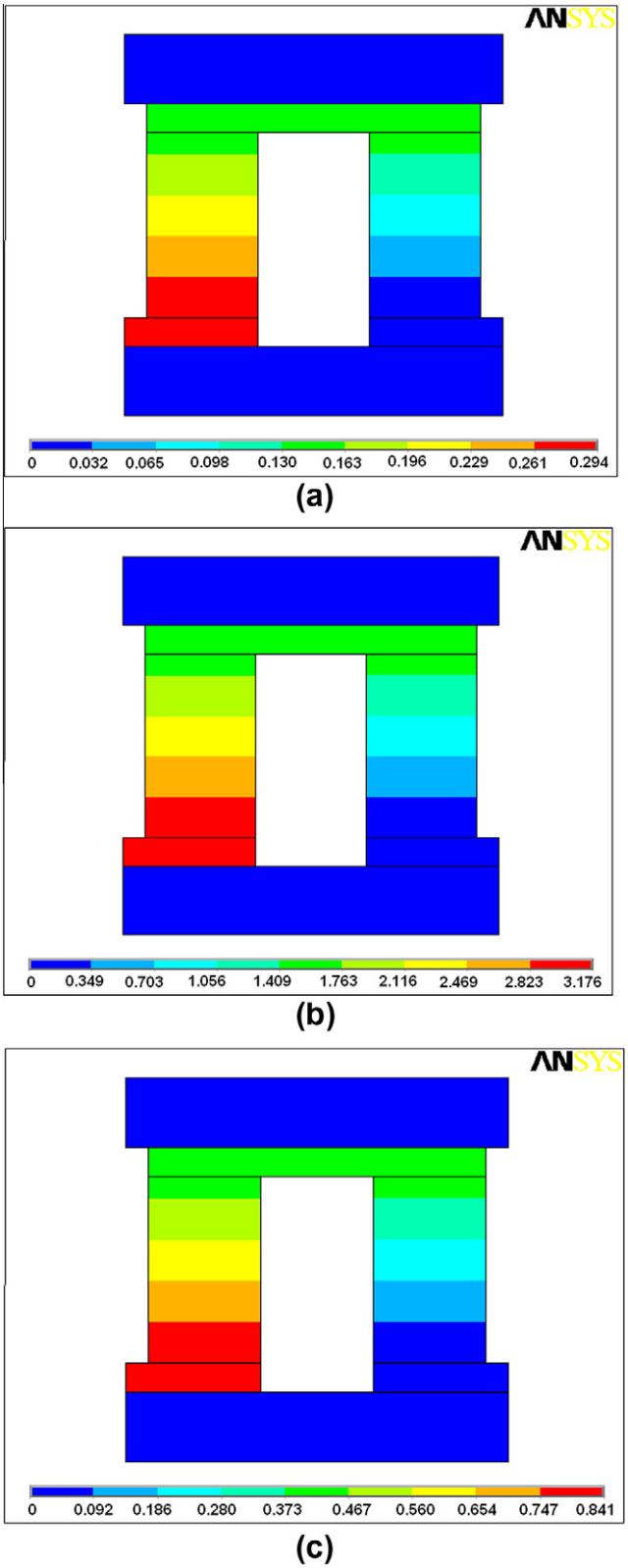

Fig. 5. Distributions of voltage for thermoelectric FEM model under different operating conditions (mV). (a) Single TEG; (b) Integrated TEG (max); and (c) Integrated TEG (stable).

3.4.4. Heat flux distribution of TEG

To investigate the distribution of heat flux on TEG, the performance of thermoelectric unicouple under above three

Table 3
Comparison between experimental and FEM simulation results of thermoelectric unicouple.

Thermoelectric unicouple	Single TEG		Integrated TEG (max)		Integrated TEG (stable)	
	Experimental	FEM	Experimental	FEM	Experimental	FEM
V_{oc} (mV)	0.295	0.294	3.189	3.176	0.846	0.841
I_{sc} (A)	0.012	0.012	0.13	0.13	0.035	0.034
$\triangle T$ (K)	2.5	2.5	27	27	7.0	7.0

Table 4
FEM simulation results (thermal input and thermal flux) of thermoelectric unicouple.

Thermoelectric unicouple	Single TEG	Integrated TEG (max)	Integrated TEG (stable)
Q_h (mW)	6.938	73.686	19.715
q_h (W/m^2)	1041.1	11057.3	2958.4

different conditions was investigated using FEM, one working individually and the other two working integrated with STC and the heat collector in HGS, namely peak condition and stable condition. The generating voltage was analyzed and the results are presented in Fig. 5. Based on the experiment and FEM simulation results, a response table was developed (Table 3). From Table 3, it can be considered that the FEM calculation solutions agreed well with the experimental results. The peak thermal input Q_h of 74 mW is obtained in the integrated TEG compared with Q_h of 7 mW in the single TEG, shown in Table 4, and the thermal input is about 20 mW in stable condition.

The heat flux vector distribution is shown in Fig. 6. It can be seen from Fig. 6a, the heat flux on the hot side of TEG is about 1000 W/m^2. However, it rises to the maximum value of 11,000 W/m^2 (Fig. 6b) and the stable value of 3000 W/m^2 (Fig. 6c) in the integrated TEG. They all accord with the values of heat flux figured out as Eq. (13), which is shown in Table 4. It indicates that much more heat is collected to the hot side of TEG owing to the design of heat collector, and the heat flux is promoted by more than tenfold after integration.

3.5. Performance of HGS

An energy utilization analysis based on energy balance and heat transfer is proposed to indicate a possible heat flux process for the HGS (Fig. 7). The solar spectrum is made up of a range of electromagnetic radiation with wavelengths mainly from 300 nm to 2500 nm, where the ultraviolet, visible and infrared light occupy 3%, 44% and 53% radiant energy, respectively. When the HGS works, sunlight falls on the surface of STC and the heat collector. STC can absorb solar light up to 800 nm, the unexploited visible light and parts of the infrared energy are transformed into the waste heat. The other solar energy is absorbed by heat collector and converted directly to heat. The waste heat from STC and the absorbed heat from the heat collector are all transferred through the copper foil to the hot side of TEG. Water cooling quickly takes heat away from the cold side of TEG. Therefore, a significant temperature difference has been created across the TEG to give high power efficiency, and the working temperature of STC also drops to show an excellent performance.

The total amount of power output can be expressed as:

$$P_{\text{tot}} = P_{\text{STC}} + P_{\text{TEG}} \tag{15}$$

where P_{STC} and P_{TEG} are the output power of STC and TEG, respectively. Then η_{STC} can be worked out as follows:

$$\eta_{\text{STC}} = \frac{P_{\text{STC}}}{G_{\text{STC}}} \times 100\% = \frac{P_{\text{STC}}}{LA_{\text{STC}}} \times 100\% \tag{16}$$

where L is the incident light intensity, A_{STC} is the illumination area on solar cell.

According to the experimental data, the performance of HGS is summarized in Table 5. When HGS works, STC, one of the components, shows stable performance for a long time. The open-circuit voltage is about 2.00 V and the short-circuit current is 220 mA, which gives a photovoltaic conversion efficiency of 4.55% according to Eq. (16). However, the performance of TEG varies according to the temperature difference across the TEG. The maximum open-circuit voltage is about 3.25 V and the short-circuit current is 260 mA. The maximum output power of TEG can reach 204 mW, which is even larger than that of STC. The total amount of generated power of 393 mW is obtained in HGS, which is increased of 107.9% compared with that of the single STC. In contrast with the previous results (Guo et al., 2010; Van Sark, 2011; Wang et al., 2011), our HGS also exhibits a larger increase rate of output power (see Table 6). These results indicate that the power generation is enhanced obviously through integrating TEC with STC and the waste heat is effectively reclaimed by TEG to give the extra electric energy. The bowl-shaped heat collector guarantees a larger temperature difference in both sides of TEG. The integration of STC and TEG in HGS shows a promising way to develop high-efficiency solar-driven power generation.

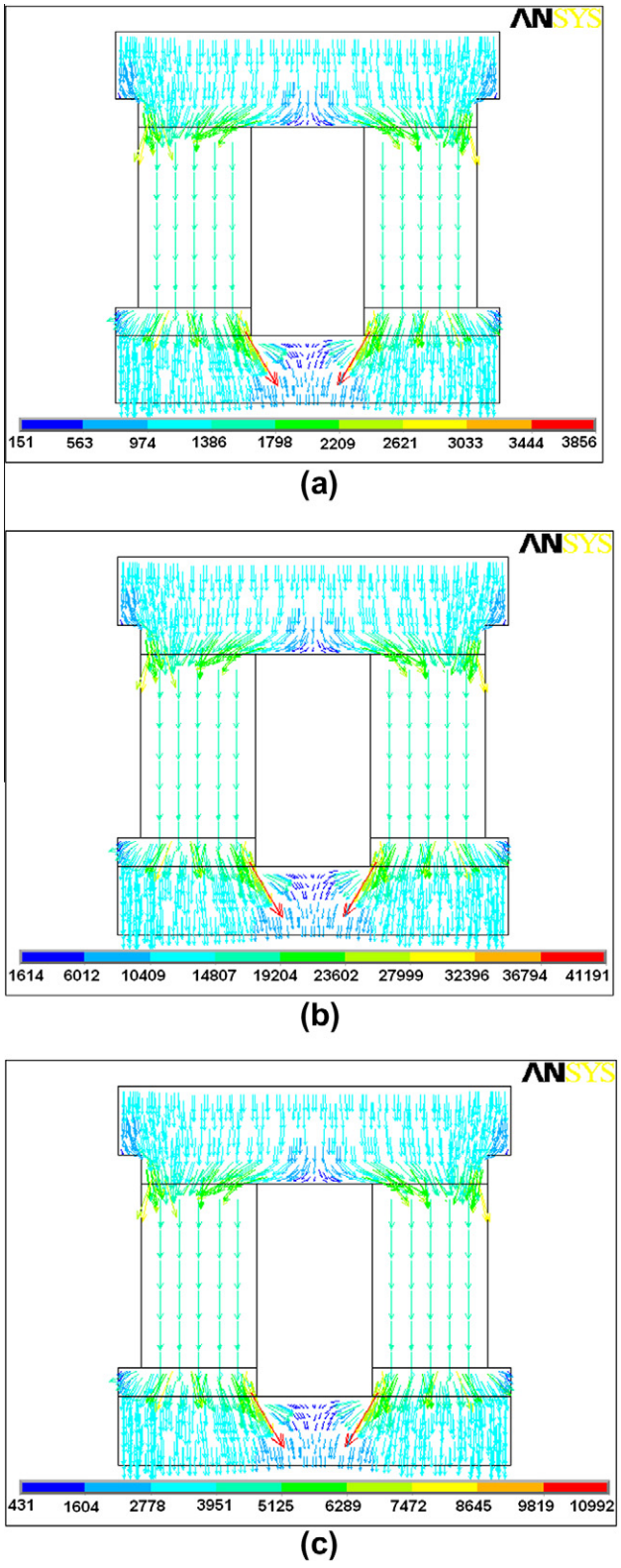

Fig. 6. Distributions of heat flux vector for thermoelectric FEM model under different operating conditions (W/m^2). (a) Single TEG; (b) Integrated TEG (max); and (c) Integrated TEG (stable).

It should be mentioned that the whole efficiency of HGS is low due to the general performance of STC and TEG. The photovoltaic conversion efficiency of the STC is only 4.55% under illumination intensity of 60 mW/cm^2. The performance of TEG greatly relies on the temperature different across the TEG. Thus, the uses of the higher ZT material for TEG and the higher efficiency PV device are alternative ways to improve the performance of HGS. In addition, optimizing thermal management design of HGS can also effectively improve the HGS generating performance.

3.6. Cost analysis

The experimental results show that the introducing of TEG into HGS benefits the performance of STC. However, it should be considered to balance the extra cost and the extra power output from TEG. Hence, a cost analysis for the model in Fig. 7 is presented to compare with STC.

The price of PV is around 4 US dollars per watt-peak of power generated (Chavez-Urbiola et al., 2012). When the heat collector is used instead of the STC, the absorber converts the solar radiation into heat and the heat is transported onto the surface of TEG by means of effective heat conduction. The advantage of the HGS is that the thermal energy in a large area can be accumulated in a small area, which is benefited for power generation of TEG. Extra cost of the heat collector (generally using solar selective absorber) should be relatively low, which is about 20 USD/m^2. As for solar thermoelectric generator, typical modules for generating electricity are found in size of 40×40 mm^2 with the cost of 60 US dollars per piece (http://www.tande.com.tw/te-power-generators.htm). It could be expected the cost for HGS could be greatly reduced when the increasing of size of the solar selective absorber and the efficiency of TEG.

Kraemer et al. (2011) have proposed a flat-panel solar thermal to electric power conversion technology based on Seebeck effect and the selective absorber, and it achieved a peak efficiency of 4.6%. Fig. 8 shows the calculated power generation cost of TEG with different efficiencies and the solar absorber areas. Here the efficiencies of 1%, 3% and 5% of TEG are chosen for the cost calculation under the standard solar irradiation of 100 W/cm^2. When the efficiency of TEG is 1% for power generation, the cost is much higher than that of PV module. Then the HGS approach (PV + TE) is economically not viable at that situation. However, the cost of TEG decreases largely with the increasing efficiency of TEG. The cost of TEG with an efficiency of 3% is comparable with that of PV module when the solar absorber area is over 0.5 m^2. At efficiency of 5% of TEG, the cost becomes even lower than 4 USD/W_P with the solar absorber area over 0.3 m^2, which is economically acceptable. The cost of HGS is cheaper than that of PV module when the solar absorber area is above 0.5 m^2 and the efficiency of TEG is above 3%. It would be more efficient than that of single PV system in large area.

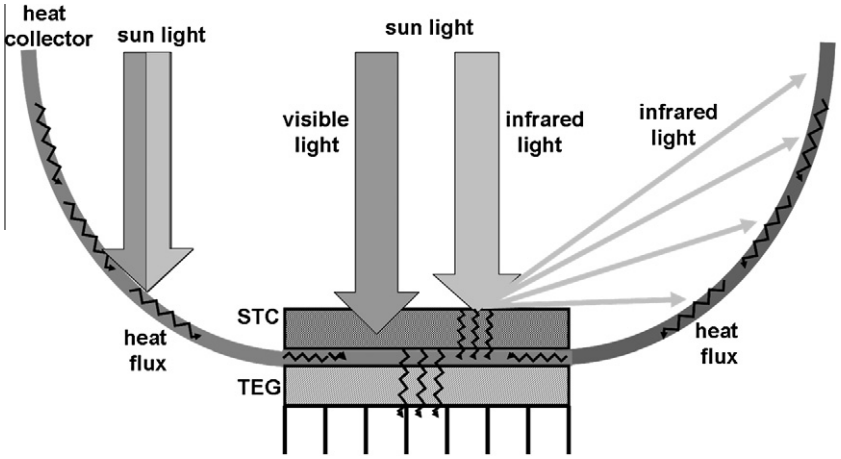

Fig. 7. Schematic diagram of heat flux in HGS.

Table 5
The performance of TEG, STC and HGS.

	FF	V_{oc} (V)		I_{sc} (A)		P_{max} (W)	
		Max	Stable	Max	Stable	Max	Stable
TEG	0.242	3.25	0.86	0.26	0.07	0.204	0.146
STC	0.430	2.00		0.22		0.189	
HGS	–	–		–		0.393	0.204

Table 6
The output power and its increase rate in HGS.

Module	P_{PV} (mW)	P_{HGS} (mW)	Increase rate (%)	Reference
STC/TEG	189	393	107.9	Our work
PV/TEG	–	–	14.7	Van Sark (2011)
DSC/TEG	9.39	13.8	46.8	Wang et al. (2011)
DSC/TEG	39.72	44.26	23	Guo et al. (2010)

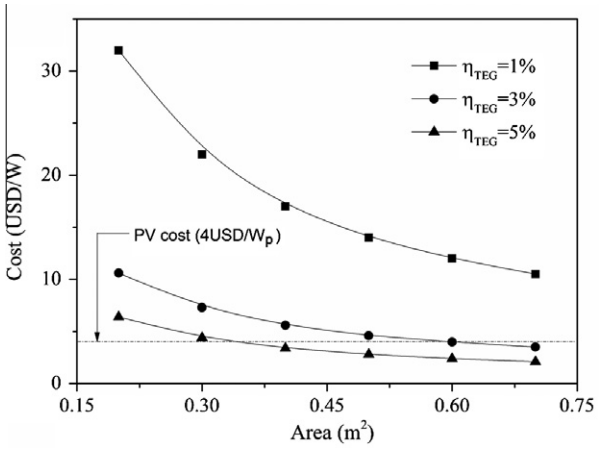

Fig. 8. Calculated power generation cost of TEG with different efficiencies and absorber areas.

4. Conclusions

A novel hybrid generation system is developed by using an integrated design to give higher power generation efficiency. The hybrid generation system consists of a silicon thin-film solar cell, thermoelectric generators and a heat collector. It is the key to design an integrated heat collector between STC and TEG which consists of the optimized absorbing layer, conducting layer and insulation layer. The absorbing layer is used to collect both solar irradiation energy and reflection energy. The insulation layer can prevent heat loss and the conducting layer ensures effective heat conduction. The hybrid design realizes the system integration and reduces energy losses. Much more heat is collected to the hot side of TEG due to the design of heat collector, and the heat flux is promoted by more than tenfold after integration according to the numerical simulation. A collaborative enhancement of output power for TEG and STC is obtained and the overall output power of sun energy has been improved by the optimized design of HGS. The total amount of generated power of HGS is enhanced to 393 mW, which is twice more than that of STC. It indicates that the HGS can effectively increase the photoelectric conversion efficiency and broaden the use of the solar spectrum. It is a promising way for the solar energy utilization with the improvement of thermoelectric device and the thermal management in HGS.

Acknowledgements

The work was supported by the State Key Development Program for Basic Research of China (Grant No. 2012CB933200), National Natural Science Foundation of China (No. 51172008 and 51002006), Beijing Technology Topic Program (No. Z111100066511009), Research Fund for Doctor Station Sponsored by the Ministry of Education of China (20111102110035) and the Fundamental Research Funds for the Central Universities.

References

Aberle, A.G., 2009. Thin-film solar cells. Thin Solid Films 517, 4706–4710.

Amatya, R., Ram, R.J., 2010. Solar thermoelectric generator for micropower applications. J. Electron. Mater. 39, 1735–1740.

Antonova, E.E., Looman, D.C., 2005. Finite elements for thermoelectric device analysis in ANSYS. In: International Conference on Thermoelectrics. Clemson, US.

Chavez-Urbiola, E.A., Vorobiev, Y.V., Bulat, L.P., 2012. Solar hybrid system with thermoelctric generators. Sol. Energy 86, 369–378.

Chen, J.C., 1996. Thermodynamic analysis of a solar-driven thermoelectric generator. J. Appl. Phys. 79, 2717–2721.

Chen, G., Dresselhaus, M.S., Dresselhaus, G., Fleuria, J.P., Caillat, T., 2003. Recent developments in thermoelectric materials. Int. Mater. Rev. 48, 1–25.

Chow, T.T., 2010. A review on photovoltaic/thermal hybrid solar technology. Appl. Energy 87, 365–379.

Crowley, T.J., 2000. Causes of climate change over the past 1000 years. Science 289, 270–277.

Deng, Y.G., Liu, J., 2009. Recent advances in direct solar thermal power generation. J. Renew. Sustain. Energy 1, 1–23.

Guo, X.Z., Zhang, Y.D., Qin, D., Luo, Y.H., Li, D.M., Pang, Y.T., Meng, Q.B., 2010. Hybrid tandem solar cell for concurrently converting light and heat energy with utilization of full solar spectrum. J. Power Sources 195, 7684–7690.

He, W., Su, Y.H., Riffat, S.B., Hou, J.X., Ji, J., 2011. Parametrical analysis of the design and performance of a solar heat pipe thermoelectric generator unit. Appl. Energy 88, 5083–5089.

Hsu, C.T., Huang, G.Y., Chu, H.S., Yu, B., Yao, D.J., 2011. Experiments and simulations on low-temperature waste heat harvesting system by thermoelectric power generators. Appl. Energy 88, 1291–1297.

Ju, X., Wang, Z.F., Flamant, G., Li, P., Zhao, W.Y., 2012. Numerical analysis and optimization of a spectrum splitting concentration phtotvoltaic–thermoelctric hybrid system. Sol. Energy 86, 1941–1954.

Kondo, M., Matsuda, A., 2004. Novel aspects in thin film silicon cells-amorphous, microcrystalline and nanocrystalline silicon. Thin Solid Film 457, 97–102.

Kraemer, D., Hu, L., Muto, A., Chen, X., Chen, G., Chiesa, M., 2008. Photovoltaic–thermoelectric hybrid systems: a general optimization methodology. Appl. Phys. Lett. 92, 243503.

Kraemer, D., Poudel, B., Feng, H.P., Caylor, J.C., Yu, B., Yan, X., Ma, Y., Wang, X.W., Wang, D.Z., Muto, A., McEnaney, K., Chiesa, M., Ren, Z.F., Chen, G., 2011. High-performance flat-panel solar thermoelectric generators with high thermal concentration. Nat. Mater. 10, 532–538.

Li, P., Cai, L.L., Zhai, P.P., Tang, X.F., Zhang, Q.J., Niino, M., 2010. Design of a concentration solar thermoelectric generator. J. Electron. Mater. 39, 1522–1530.

Muhtaroglu, A., Yokochi, A., Jouanne, A.V., 2008. Integration of thermoelectrics and photovoltaics as auxiliary power sources in mobile computer application. J. Power Sources 177, 239–246.

Omer, S.A., Infield, D.G., 2000. Design and thermal analysis of a two stage solar concentrator for combined heat and thermoelectric power generation. Energy Convers. Manage. 41, 737–756.

Rockendorf, G., Sillmann, R., Podlowski, L., Litzenburger, B., 1999. PV-hybrid and thermoeletric collectors. Sol. Energy 67, 227–237.

Sark, W., 2011. Feasibility of photovoltaic–thermoelectric hybrid modules. Appl. Energy 88, 2785–2790.

Vorobiev, Y., Gonzalez-Hernandez, J., Vorobiev, P., Bulat, L., 2006. Thermal–photovoltaic solar hybrid system for efficient solar energy conversion. Sol. Energy 80, 170–176.

Wang, N., Han, L., He, H.C., Park, N.H., Koumoto, K., 2011. A novel high-performance photovoltaic–thermoelectric hybrid device. Energy Environ. Sci. 4, 3676–3679.

Xiao, J.S., Yang, T.Q., Li, P., Zhai, P.C., Zhang, Q.J., 2011. Thermal design and management for performance optimization of solar thermoelectric generator. Appl. Energy 93, 33–38.

Yamamoto, K., Nakajima, A., Yoshimi, M., Sawada, T., Fukuda, S., Suezaki, T., Ichikawa, M., Koi, Y., Goto, M., Meguro, T., Matsuda, T., Kondo, M., Sasaki, T., Tawada, Y., 2004. A high efficiency thin film silicon solar cell and module. Sol. Energy 77, 939–949.

Yang, D.J., Yin, H.M., 2011. Energy conversion efficiency of a novel hybrid solar system for photovoltaic, thermoelectric, and heat utilization. Ieee Trans. Energy Convers. 26, 662–670.

Yu, H.Y., Li, Y.Q., Shang, Y.H., Su, B., 2008. Design and investigation of photovoltaic and thermoelectric hybrid power source for wireless sensor networks. In: The 3rd IEEE International Conference on Nano/Micro Engineered and Molecular Systems. Sanya, China.